

Score Combining for Contrastive OOD Detection

Edward T. Reehorst

*Sensors Directorate
Air Force Research Lab
Wright-Patterson Air Force Base, OH 45433-7320, USA*

EDWARD.REEHORST@US.AF.MIL

Philip Schniter

*Department of Electrical and Computer Engineering
The Ohio State University
Columbus, OH 43210, USA*

SCHNITER.1@OSU.EDU

Abstract

In out-of-distribution (OOD) detection, one is asked to classify whether a test sample comes from a known inlier distribution or not. We focus on the case where the inlier distribution is defined by a training dataset and there exists no additional knowledge about the novelties that one is likely to encounter. This problem is also referred to as novelty detection, one-class classification, and unsupervised anomaly detection. The current literature suggests that contrastive learning techniques are state-of-the-art for OOD detection. We aim to improve on those techniques by combining/ensembling their scores using the framework of null hypothesis testing and, in particular, a novel generalized likelihood ratio test (GLRT). We demonstrate that our proposed GLRT-based technique outperforms the state-of-the-art CSI and SupCSI techniques from (Tack et al., 2020) in dataset-vs-dataset experiments with CIFAR-10, SVHN, LSUN, ImageNet, and CIFAR-100, as well as leave-one-class-out experiments with CIFAR-10. We also demonstrate that our GLRT outperforms the score-combining methods of Fisher, Bonferroni, Simes, Benjamini-Hochwald, and Stouffer in our application.

Keywords: Out-of-distribution detection, contrastive learning, hypothesis testing

1 Introduction

Out-of-distribution (OOD) detection refers to the problem of classifying whether a test sample comes from a known *inlier* distribution or not. OOD detection has wide-ranging applications in, e.g., intrusion detection in cybersecurity; fraud detection in finance, insurance, healthcare, and telecommunications; industrial fault and damage detection; monitoring of infrastructure and stock markets; acoustic novelty detection; medical diagnosis and disease outbreak detection; even detection in the earth sciences; and scientific discovery in chemistry, bioinformatics, genetics, physics, and astronomy—see the recent comprehensive overview (Ruff et al., 2021) for specific citations.

We focus on the case where the inlier distribution is defined by a dataset $\mathcal{X} = \{\mathbf{x}_i\}$ and there is no prior knowledge about non-inlier samples. In the literature, this problem is also referred to as unsupervised anomaly detection, novelty detection, one-class classification, and open-set classification (Ruff et al., 2021). Although semi-supervised variations of OOD detection have been proposed using, e.g., outlier exposure (Hendrycks et al., 2019a; Ruff et al., 2020) and transfer learning with pre-trained networks (Reiss et al., 2021; Deecke et al., 2021; Reiss and Hoshen, 2023), we focus on the purely unsupervised setting.

Many methods have been developed for OOD detection. Among classical approaches, there are those based on density estimation, e.g., using Mahalanobis distance (Laurikkala et al., 2000), Gaussian mixture models (GMMs) (Bishop, 1994), nearest-neighbor distance (Ramaswamy et al., 2000; Breunig et al., 2000), or kernel density estimation (KDE) (Latecki et al., 2007). However, the density estimation is fundamentally difficult with high-dimensional data, such as images, due to the curse of dimensionality (Zimek et al., 2012). There also exist classical approaches based on kernel PCA (Hoffmann, 2007) and support vector machines (SVMs) (Schölkopf et al., 2001; Tax and Duin, 2004), but selecting kernels and hand-crafting relevant features is challenging. For example, many contemporary OOD detection tasks aim to distinguish high-level semantic differences (e.g., objects from non-normal classes) over low-level sensory differences (e.g., texture defects) (Ahmed and Courville, 2020). In the raw feature space, semantic novelties can be very close to inliers according to traditional ℓ_p and kernel-based distances. For example, an image of a dog with fur that is cat-like fur texture and color similar to a cat can be more similar in raw pixel space than various cat breeds among themselves.

To address the shortcomings of these classical approaches, a wide variety of deep neural network (DNN)-based OOD detection techniques have been proposed. As described in recent surveys (Chalapathy and Chawla, 2019; Di Mattia et al., 2019; Pang et al., 2021; Ruff et al., 2021), they include methods based on deep autoencoders, deep SVMs, deep generative networks, such as generative adversarial networks and normalizing flows, and self-supervised methods. Among these, self-supervised methods like the contrastive shifted instances (CSI) (Tack et al., 2020) have been particularly effective, perhaps because self-supervised learning seems to exhibit inductive biases towards semantic representations (Ahmed and Courville, 2020).

Most OOD detection techniques construct an *inlier score* that quantifies how likely a given sample is to be an inlier. A test sample is classified as an inlier if its score exceeds a predetermined threshold. In some cases, several intermediate scores are computed and then combined to form the final score. For example, with self-supervised techniques, it’s common to compute intermediate scores using pretext tasks, augmented views, and/or distribution shifts (Golan and El-Yaniv, 2018; Hendrycks et al., 2019b; Bergman and Hoshen, 2020; Tack et al., 2020; Georgescu et al., 2021; Khalid et al., 2022). However, the score combining methodologies in these works are heuristic. Our contributions are as follows.

1. We propose to use the framework of null-hypothesis testing to design principled score-combining techniques for self-supervised OOD detection.
2. We propose a novel score-combining technique based on a generalized likelihood ratio test (GLRT), and we demonstrate that it performs better than the classical Fisher, Bonferroni, Simes/Benjamini-Hochwald (BH), Stouffer, and ALR tests in our application.
3. We show how to achieve false-alarm-rate guarantees with a finite-sample validation set.
4. We demonstrate improvements over the state-of-the-art CSI and SupCSI (Tack et al., 2020) contrastive OOD detectors on dataset-vs-dataset experiments with CIFAR-10,

SVHN, LSUN, ImageNet, and CIFAR-100 and on leave-one-class-out experiments with CIFAR-10.

To our knowledge, this is the first work to apply the null-hypothesis testing framework to self-supervised OOD detection. Null-hypothesis testing has been applied to other forms of OOD detection, though. For example, Bergamin et al. (2022) used Fisher’s method combine two scores produced by deep generative models. Kaur et al. (2022) aggregated conformity scores measuring transformational equivariance into a single p-value, which was thresholded for OOD detection. Haroush et al. (2022) computed p-values for each class, layer, and channel in a DNN trained for supervised classification, and combined those scores into a final p-value using a combination of Fisher’s and Simes’ methods. Magesh et al. (2022) used the BH procedure (Benjamini and Hochberg, 1995) to aggregate scores from the feature maps of a DNN trained for supervised classification in a way that yields guarantees on the false-alarm rate. Note that, in (Haroush et al., 2022) and (Magesh et al., 2022), the goal was to determine whether a *given* trained DNN behaves differently on a test sample compared to the samples used to train it. However, depending on how it was trained, that DNN could throw away information that is useful for OOD detection. Our approach is different: Given an inlier dataset \mathcal{X} , we aim to design/train a DNN to detect whether a test sample is OOD or not.

2 Background

2.1 Self-supervised learning for OOD detection

There are two main approaches to self-supervised learning (Ericsson et al., 2022). The first is to design a pretext task that yields a set of labels and then use those labels to train a DNN in a supervised manner. An example is training a DNN to predict the rotation of an image by either 0, 90, 180, or 270 degrees (Gidaris et al., 2018). The intermediate features of the trained DNN can then be used for other tasks, such as OOD detection (Golan and El-Yaniv, 2018; Hendrycks et al., 2019b; Bergman and Hoshen, 2020). When the dimensionality of these features is sufficiently small, classical approaches to OOD detection are effective.

The other main approach to self-supervised learning is contrastive learning, which trains the DNN to distinguish between semantically similar augmented views of a given data sample and other data samples. Concretely, let $A_0(\cdot)$ and $A_1(\cdot)$ denote two augmentations randomly selected from an augmentation set \mathcal{A} (e.g., for images, crop, horizontal flip, color jitter, and grayscale, as in (Tack et al., 2020)), and let $\mathbf{g}_\theta(A_a(\mathbf{x}_i))$ for $a \in \{0, 1\}$ be the corresponding augmented outputs from DNN $\mathbf{g}_\theta(\cdot)$. Using the shorthand $\mathbf{g}_i^a \triangleq \mathbf{g}_\theta(A_a(\mathbf{x}_i))$, and denoting cosine similarity by

$$\text{sim}(\mathbf{g}_i, \mathbf{g}_{i'}) \triangleq \frac{\mathbf{g}_i^\top \mathbf{g}_{i'}}{\|\mathbf{g}_i\| \|\mathbf{g}_{i'}\|}, \quad (1)$$

contrastive learning trains θ to maximize $\text{sim}(\mathbf{g}_i^0, \mathbf{g}_i^1)$ while minimizing $\text{sim}(\mathbf{g}_i^a, \mathbf{g}_{i'}^{a'})$ for $(i', a') \neq (i, a)$. For example, SimCLR (Chen et al., 2020) trains θ to minimize $\mathcal{L}_{\text{con}}(\theta)$

over a B -sample batch, where

$$\mathcal{L}_{\text{con}}(\boldsymbol{\theta}) = \frac{1}{2B} \sum_{i=1}^B \sum_{a=0}^1 -\ln \frac{\exp(\text{sim}(g_{\boldsymbol{\theta}}(\mathbf{x}_i^a), g_{\boldsymbol{\theta}}(\mathbf{x}_i^{1-a}))/\tau)}{\sum_{(i',a') \neq (i,a)} \exp(\text{sim}(g_{\boldsymbol{\theta}}(\mathbf{x}_i^a), g_{\boldsymbol{\theta}}(\mathbf{x}_{i'}^{a'}))/\tau)} \quad (2)$$

and $\tau > 0$ is a tunable temperature. Once trained, the outputs and/or intermediate-layer features of $g_{\boldsymbol{\theta}}(\cdot)$ can be employed for OOD detection using classical methods. For example, Winkens et al. (2020) used Mahalanobis distance while Sohn et al. (2021) used KDE and one-class SVM (OC-SVM).

SimCLR drives the inlier features $\{g_i^a\}$ towards a uniform distribution on the hypersphere (Wang and Isola, 2020), which makes it difficult to distinguish inliers from OOD samples. Thus, Tack et al. (2020) and Sohn et al. (2021) proposed to augment the data $\{\mathbf{x}_i\}$ using *distribution-shifting transformations* $T_j(\cdot) \in \mathcal{T}$, such as $\{0^\circ, 90^\circ, 180^\circ, 270^\circ\}$ image rotations.

The contrastive shifted instances (CSI) technique from (Tack et al., 2020) achieves state-of-the-art performance by training with a loss that combines SimCLR with distribution-shift prediction. Once the DNN $g_{\boldsymbol{\theta}}(\cdot)$ is trained, CSI evaluates and combines $3|\mathcal{T}| = 12$ different scores for the above shift set \mathcal{T} . Some scores are computed from the outputs of $g_{\boldsymbol{\theta}}(\cdot)$ and others from the logits $w(\mathbf{x}) \in \mathbb{R}^{|\mathcal{T}|}$ of a linear shift-classifier head that is attached at $f_{\boldsymbol{\theta}}(\cdot)$, which is two layers behind the output of $g_{\boldsymbol{\theta}}(\cdot)$. CSI uses three base scores:

$$s_{\text{cos},j}(\mathbf{x}) \triangleq \max_{\mathbf{x}' \in \mathcal{X}_{\text{train}}} \text{sim}(g_{\boldsymbol{\theta}}(R_j(\mathbf{x})), g_{\boldsymbol{\theta}}(R_j(\mathbf{x}')))) \quad (3)$$

$$s_{\text{norm},j}(\mathbf{x}) \triangleq \|g_{\boldsymbol{\theta}}(R_j(\mathbf{x}))\| \quad (4)$$

$$s_{\text{shift},j}(\mathbf{x}) \triangleq w_j(R_j(\mathbf{x})), \quad (5)$$

defined for shifts $j \in \{1, \dots, |\mathcal{T}|\}$, and then combines them into a single score as follows:

$$s_{\text{CSI}}(\mathbf{x}) \triangleq \sum_{j=1}^{|\mathcal{T}|} \left[\lambda_j^{\text{con}} s_{\text{cos},j}(\mathbf{x}) s_{\text{norm},j}(\mathbf{x}) + \lambda_j^{\text{shift}} s_{\text{shift},j}(\mathbf{x}) \right] \quad (6)$$

$$\lambda_j^{\text{con}} \triangleq \left[\frac{1}{n} \sum_{i=1}^n s_{\text{norm},j}(\mathbf{x}_i) \right]^{-1} \quad \text{and} \quad \lambda_j^{\text{shift}} \triangleq \left[\frac{1}{n} \sum_{i=1}^n s_{\text{shift},j}(\mathbf{x}_i) \right]^{-1}. \quad (7)$$

When the inlier dataset $\{\mathbf{x}_i\}$ has class labels $y_i \in \{1, \dots, K\}$, SupCSI (Tack et al., 2020) exploits them to outperform CSI. SupCSI trains with SupCLR (Khosla et al., 2020) instead of SimCLR, as well as joint class/shift prediction. Once the DNN is trained, the class/shift logits $\boldsymbol{\ell}^{K \times |\mathcal{T}|}(\cdot)$ are used to construct the score

$$s_{\text{SupCSI}}(\mathbf{x}) = \max_{k=1, \dots, K} \left[\text{softmax} \left(\frac{1}{|\mathcal{T}|} \sum_{j=1}^{|\mathcal{T}|} \boldsymbol{\ell}_{:,j}(R_j(\mathbf{x})) \right) \right]_k, \quad (8)$$

where $\boldsymbol{\ell}_{:,j}(\cdot)$ is the j th column of $\boldsymbol{\ell}(\cdot)$ and $[\text{softmax}(\boldsymbol{\ell})]_k \triangleq \exp(\ell_k) / \sum_{k'=1}^K \exp(\ell_{k'})$. Although CSI and SupCSI yield state-of-the-art performance, their score-combining rules (6)-(8) are heuristic, leaving room for improvement. Also, it's not clear how additional scores could be incorporated into (6)-(8).

2.2 Statistical hypothesis testing for OOD detection

Null hypothesis testing. Consider the problem of choosing between two hypotheses, H_0 (null) and H_1 (alternative), where H_0 says that \mathbf{x} was drawn from some distribution $P_{\mathbf{x}}$ and H_1 says that it was not drawn from $P_{\mathbf{x}}$. Applied to OOD detection, \mathbf{x} is an inlier under H_0 and an OOD sample under H_1 . Given a test statistic $s(\mathbf{x})$ that measures confidence in H_0 (i.e., an *inlier score*), we reject the null hypothesis when $s(\mathbf{x}) \leq \tau$ for some threshold τ . A false alarm, or *type-1* error, occurs when we mistakenly reject an \mathbf{x} generated under H_0 . The probability of a false alarm, $\alpha = \Pr\{s(\mathbf{X}) \leq \tau \mid H_0\}$, is known as the *significance level*. Usually, α is determined by the application and τ is adjusted accordingly.

Often, *p-values* are used to quantify the significance of a test outcome. For an observed $s = s(\mathbf{x})$, the p-value is defined as follows, where \mathbf{X} denotes a random version of \mathbf{x} :

$$q(s) \triangleq \Pr\{s(\mathbf{X}) \leq s \mid H_0\}. \quad (9)$$

The p-value indicates the probability of observing a test outcome that is equal or more extreme than s given that H_0 is true. If we treat s as a random variable (i.e., $S \triangleq s(\mathbf{X})$ for random test sample \mathbf{X}), and assume that the cumulative distribution function (cdf) of S under H_0 is continuous, then $q(S)$ is uniformly distributed on $[0, 1]$ under the null hypothesis (Wasserman, 2004), i.e., $\Pr\{q(S) \leq \alpha \mid H_0\} = \alpha$ for any $\alpha \in (0, 1)$. So, given an observed s , to reject the null hypothesis at a significance of α , we simply check whether $q(s) \leq \alpha$.

Global null tests. Suppose that we have access to $m > 1$ statistics $\{s_l(\mathbf{x})\}_{l=1}^m$ of the form described above, and that we associate them with the respective hypothesis pairs $\{H_{0l}, H_{1l}\}_{l=1}^m$. The *global null hypothesis* refers to the case where all null hypotheses are true, i.e., $H_0 = \bigcap_{l=1}^m H_{0l}$. Because the statistics $\{s_l(\mathbf{x})\}$ can differ significantly over l , it's much easier to combine them after they have been converted to p-values $\mathbf{q} = [q_1, \dots, q_m]^\top$.

Famous methods for combining p-values include Fisher's method (Fisher, 1992), Bonferroni's method (Wasserman, 2004), Sime's method (Simes, 1986), and the BH procedure (Benjamini and Hochberg, 1995). Each method is associated with a test statistic $t(\mathbf{q})$ that rejects the global null H_0 when $t(\mathbf{q}) \leq \tau$, for an appropriately chosen threshold τ . These statistics can be written as

$$t_{\text{fisher}}(\mathbf{q}) \triangleq \sum_{l=1}^m \ln q_l \quad (10)$$

$$t_{\text{bon}}(\mathbf{q}) \triangleq \min_l q_l \quad (11)$$

$$t_{\text{simes}}(\mathbf{q}) = t_{\text{BH}}(\mathbf{q}) \triangleq \min_l q_{(l)}/l, \quad (12)$$

where $q_{(l)}$ is the l th sorted p-value such that $q_{(1)} \leq q_{(2)} \leq \dots \leq q_{(m)}$.

3 Proposed method

Suppose we have m inlier score functions $\{s_l(\cdot)\}_{l=1}^m$, where $s_l : \mathbb{R}^d \rightarrow \mathbb{R}$ and a larger value of $s_l(\mathbf{x})$ indicates increasing confidence in hypothesis H_0 , i.e., that \mathbf{x} is an inlier. As described in Section 2.1, such scores commonly arise in self-supervised OOD detectors. Our goal is

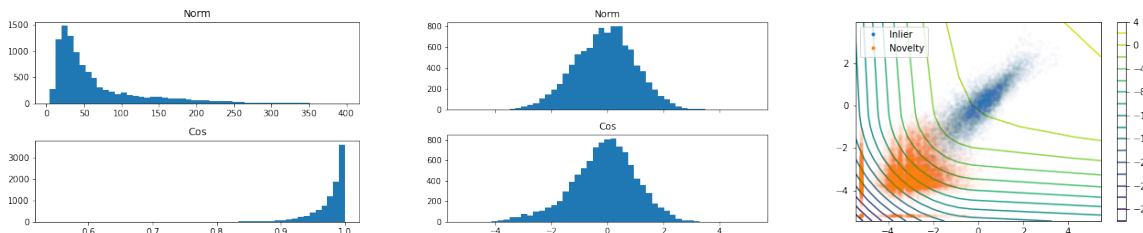


Figure 1: Left: Histogram of CSI’s “norm” score $\{s_1(\mathbf{x}_i)\}_{i=1}^n$ (top) and “cos” score $\{s_2(\mathbf{x}_i)\}_{i=1}^n$ (bottom) for CIFAR-10 inliers $\mathcal{X}_{\text{test}}^{\text{cifar10}}$. Center: Histograms of the corresponding empirical z-values $\{\hat{z}_1(s_1(\mathbf{x}_i))\}_{i=1}^n$ and $\{\hat{z}_2(s_2(\mathbf{x}_i))\}_{i=1}^n$ with $\hat{z}_1(\cdot)$ and $\hat{z}_2(\cdot)$ constructed using CIFAR-10 inliers $\mathcal{X}_{\text{train}}^{\text{cifar10}}$. Right: Scatter plot of $\hat{z}_1(s_1(\mathbf{x}_i))$ (horizontal axis) versus $\hat{z}_2(s_2(\mathbf{x}_i))$ (vertical axis) for CIFAR-10 inliers $\mathcal{X}_{\text{test}}^{\text{cifar10}}$ and SVHN novelties $\mathcal{X}_{\text{test}}^{\text{svhn}}$. Contours show the value of the proposed GLRT score $t_{\text{GLRT}}(\mathbf{z})$ versus z_1 and z_2 .

to combine these m scores $\{s_l(\mathbf{x})\}$ into a single test statistic $t(\mathbf{x})$ that we can threshold via $t(\mathbf{x}) \leq \tau$ to classify whether \mathbf{x} is an inlier or not.

One of the main challenges in combining scores is that they can have very different distributions (see the left pane of Figure 1). If the scores were simply summed together, the larger scores could overwhelm the smaller ones, regardless of whether they were more informative or not. As discussed in Section 2.2, a common way to circumvent this problem is to transform each score $s_l(\mathbf{x})$ to its p-value $q_l(s_l(\mathbf{x}))$ and combine the p-values using, e.g., Bonferroni, Fisher, or Simes/BH.

Another principled approach to combining scores uses *z-values*,

$$z_l(s) \triangleq \Phi^{-1}(q_l(s)) \text{ for p-value } q_l(s) \text{ and the standard-normal cdf } \Phi(\cdot), \quad (13)$$

which are standard-normal distributed under H_0 rather than uniform; see (Cousins, 2007) for a historical perspective; Because $s_l(\mathbf{x})$ is an inlier score and $z_l(s)$ is monotonically increasing in s , we can also interpret $z_l(s_l(\mathbf{x}))$ as an inlier score. A well-known way to combine z-values $\mathbf{z} = [z_1, \dots, z_m]^\top$ is to use *Stouffer’s statistic*,

$$t_{\text{stouffer}}(\mathbf{z}) \triangleq \frac{1}{\sqrt{m}} \sum_{l=1}^m z_l, \quad (14)$$

which we evaluate in Section 4. Below, we propose a different way to combine z-values.

In the sequel, when dealing with random \mathbf{X} , we will abbreviate $z_l(s_l(\mathbf{X}))$ as Z_l , which is itself random, and define $\mathbf{Z} \triangleq [Z_1, \dots, Z_m]^\top$. Likewise, for a deterministic observed test sample \mathbf{x} , we will abbreviate $z_l(s_l(\mathbf{x}))$ as z_l , which is itself deterministic, and define $\mathbf{z} \triangleq [z_1, \dots, z_m]^\top$.

3.1 The negative-means problem and a GLRT-based solution

We formulate OOD detection as the following hypothesis testing problem:

$$H_0 : \mathbf{Z} \sim \mathcal{N}(\mathbf{0}, \mathbf{I}) \quad (15a)$$

$$H_1 : \mathbf{Z} \sim \mathcal{N}(\boldsymbol{\mu}, \mathbf{I}) \text{ with } \mu_l \leq -\epsilon \text{ for all } l = 1, \dots, m, \quad (15b)$$

which we will refer as the *negative-means* (NM) problem. Here, the constant $\epsilon > 0$ is specified in advance but $\boldsymbol{\mu} = [\mu_1, \dots, \mu_m]^\top$ is unknown. The motivation for (15a) is that, by construction, each Z_l is standard-normal under H_0 . The motivation for (15b) is that, because each z_l constitutes an inlier score, the (unknown) mean of Z_l under H_1 should be ϵ less than the mean of Z_l under H_0 , for some $\epsilon > 0$. To be clear, (15) models the z -values as independent, even though we don't expect this property to hold in practice. We discuss alternative formulations that circumvent this independence assumption in Appendix A.

If $\boldsymbol{\mu}$ in (15) was known, we could solve (15) using a likelihood ratio test (LRT) (Lehmann et al., 2005), i.e.,

$$\text{LR}(\mathbf{z}) \underset{H_1}{\overset{H_0}{\geq}} \tau' \quad \text{for} \quad \text{LR}(\mathbf{z}) \triangleq \frac{p(\mathbf{z}|H_0)}{p(\mathbf{z}|H_1)}, \quad (16)$$

where $p(\mathbf{z}|H_i)$ denotes the probability density function (pdf) of \mathbf{Z} under H_i . The LRT is known to be Neyman-Pearson optimal, meaning that the probability of detection is maximized for a fixed false-alarm rate (Lehmann et al., 2005). Thresholding $\text{LR}(\mathbf{z})$ in (16) would be equivalent to thresholding the log-LR

$$\ln \text{LR}(\mathbf{z}) = -\frac{1}{2}\|\mathbf{z}\|^2 + \frac{1}{2}\|\mathbf{z} - \boldsymbol{\mu}\|^2 = -\boldsymbol{\mu}^\top \mathbf{z} + \frac{1}{2}\|\boldsymbol{\mu}\|^2, \quad (17)$$

and thus equivalent to thresholding $-\boldsymbol{\mu}^\top \mathbf{z}$ at some τ .

In (15), however, $\boldsymbol{\mu}$ is unknown, and thus (15) is a *composite* hypothesis testing problem (Lehmann et al., 2005). For such problems, a *uniformly most powerful* (UMP) test exists when there exists a Neyman-Pearson test statistic that is invariant to the unknown parameters (Lehmann et al., 2005). In our case, because the test statistic $-\boldsymbol{\mu}^\top \mathbf{z}$ depends on the direction of the unknown $\boldsymbol{\mu}$, a UMP does not exist unless $m = 1$. When $m = 1$, because $-\mu_1 \geq \epsilon > 0$, we can form a UMP test by rejecting H_0 whenever $z_1 \leq \tau$.

A common approach to composite hypothesis testing is the generalized LRT (GLRT) (Lehmann et al., 2005). For the NM problem (15), the GLRT takes the form

$$\text{GLR}(\mathbf{z}) \underset{H_1}{\overset{H_0}{\geq}} \tau' \quad \text{for} \quad \text{GLR}(\mathbf{z}) \triangleq \frac{p(\mathbf{z}|H_0)}{\max_{\boldsymbol{\mu}: \mu_l \leq -\epsilon \forall l} p(\mathbf{z}|H_1, \boldsymbol{\mu})}. \quad (18)$$

Wei et al. (2019) studied (18) when $\epsilon = 0$, in which case the set $\{\boldsymbol{\mu} : \mu_l \leq -\epsilon \forall l\}$ is a closed convex cone. For that case, they proved that the GLRT is optimal in a minimax sense. We focus on the case that $\epsilon > 0$, which tends to improve performance in our application, as shown in Section 4.

To simplify the GLRT (18), we first derive the denominator-maximizing value of $\boldsymbol{\mu}$ as

$$\arg \max_{\boldsymbol{\mu}: \mu_l \leq -\epsilon \forall l} p(\mathbf{z}|H_1, \boldsymbol{\mu}) = \arg \min_{\boldsymbol{\mu}: \mu_l \leq -\epsilon \forall l} \|\mathbf{z} - \boldsymbol{\mu}\|^2 = \mathbf{z}^- \quad \text{for} \quad [\mathbf{z}^-]_l = z_l^- \triangleq \min\{z_l, -\epsilon\} \quad . \quad (19)$$

Then we plug this value of $\boldsymbol{\mu}$ into the log-LR expression (17) to obtain the log-GLR

$$\ln \text{GLR}(\mathbf{z}) = -(\mathbf{z}^-)^\top \mathbf{z} + \frac{1}{2}\|\mathbf{z}^-\|^2 = (\frac{1}{2}\mathbf{z}^- - \mathbf{z})^\top \mathbf{z}^- \triangleq t_{\text{GLRT}}(\mathbf{z}), \quad (20)$$

which we use as our proposed test statistic. In other words, we reject the null hypothesis H_0 whenever $t_{\text{GLRT}}(\mathbf{z}) \leq \tau$ for some appropriately chosen threshold τ .

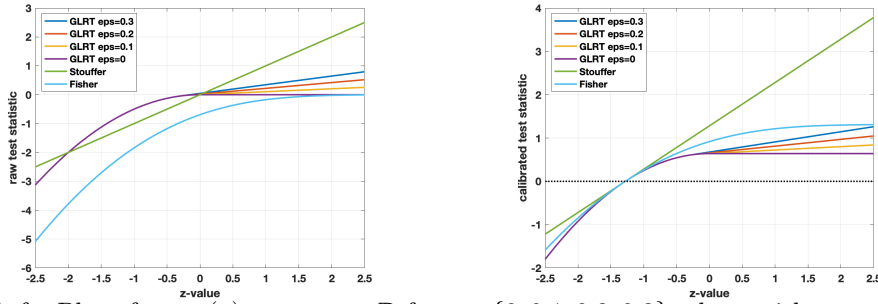


Figure 2: Left: Plot of $t_{\text{GLRT}}(z)$ versus $z \in \mathbb{R}$ for $\epsilon \in \{0, 0.1, 0.2, 0.3\}$, along with $t_{\text{stouffer}}(z) = z$ and $t_{\text{fisher}}(z) = \ln \Phi(z)$. Right: a plot of the same test statistics after shifting and scaling $t(z)$ so that $\Pr\{t(z) \leq 0 \mid H_0\} = 0.1$ and $t'(z_0) = 1$ for z_0 such that $t(z_0) = 0$.

Algorithm 1 The proposed GLRT-based OOD detector for a given threshold τ

Require: test sample \mathbf{x} , test threshold τ , training samples $\{\mathbf{x}_i\}_{i=1}^n$, scores $\{s_l(\cdot)\}_{l=1}^m$, NM parameter $\epsilon > 0$.

- 1: $\forall l = 1, \dots, m : \hat{F}_l(\mathbf{x}) = \frac{1}{n} \sum_{i=1}^n \mathbf{1}\{s_l(\mathbf{x}_i) \leq s_l(\mathbf{x})\}$
 - 2: $\forall l = 1, \dots, m : \hat{z}_l(\mathbf{x}) = \Phi^{-1}(\hat{F}_l(\mathbf{x}))$
 - 3: $t_{\text{GLRT}}(\mathbf{x}) = \sum_{l=1}^m \left(\frac{1}{2}\hat{z}_l^-(\mathbf{x}) - \hat{z}_l(\mathbf{x})\right)\hat{z}_l^-(\mathbf{x})$ for $\hat{z}_l^-(\mathbf{x}) = \min\{\hat{z}_l(\mathbf{x}), -\epsilon\}$
 - 4: **return** “OOD” if $t_{\text{GLRT}}(\mathbf{x}) \leq \tau$, else “inlier.”
-

In Figure 2(a), we plot $t_{\text{GLRT}}(z)$ versus $z \in \mathbb{R}$ for $\epsilon \in \{0, 0.1, 0.2, 0.3\}$, for comparison to $t_{\text{stouffer}}(z) = z$ and $t_{\text{fisher}}(z) = \ln \Phi(z)$. To facilitate an easier visual comparison, we exploit the fact that the test $t(z) \leq \tau$ is equivalent to $\bar{t}(z) \triangleq C(t(z) - \tau) \leq 0$ for any constant $C > 0$. We then choose (C, τ) to calibrate each test so that $\Pr\{\bar{t}(z) \leq 0 \mid H_0\} = 0.1$ (i.e., each test has a false-alarm rate of 0.1) and $\bar{t}'(z_0) = 1$ for z_0 such that $\bar{t}(z_0) = 0$ (i.e., each test has unit slope at the false-alarm threshold). We plot the calibrated tests in Figure 2(b).

3.2 Empirical z-values

In practice, it’s not possible to compute the z-value in (13) because we don’t know the cdf of $s_l(\mathbf{X})$ under H_0 . Thus we propose to use *empirical z-values*, which are computed from training data $\mathcal{X}_{\text{train}} = \{\mathbf{x}_i\}_{i=1}^n$ via

$$\hat{z}_l(s) \triangleq \Phi^{-1}(\hat{F}_l(s)), \quad \hat{F}_l(s) \triangleq \frac{1}{n} \sum_{i=1}^n \mathbf{1}\{s_l(\mathbf{x}_i) \leq s\}, \quad (21)$$

where $\mathbf{1}(\cdot)$ is the indicator function and $\hat{F}_l(\cdot)$ is the empirical cdf of $\{s_l(\mathbf{x}_i)\}_{i=1}^n$. See the middle plot of Figure 1 for an example.

For the case of a given threshold τ , we summarize the proposed OOD detector in Algorithm 1 using a streamlined notation that writes the z-values $\hat{z}_l(s(\mathbf{x}))$ and GLRT score $t_{\text{GLRT}}(\mathbf{z}(\mathbf{x}))$ directly as functions of \mathbf{x} .

It is not immediately obvious, though, how to choose the threshold τ when the goal is to achieve a target false-alarm rate of α . Doing so is the subject of the next section.

3.3 False-alarm-rate guarantees

In this section we consider how to guarantee a target false-alarm rate of α for a statistical test $t(\cdot)$ that rejects H_0 when $t(\mathbf{x}) \leq \tau$ for some threshold τ . Ideally, we would like to choose τ such that the false-alarm rate $\Pr\{t(\mathbf{X}) \leq \tau | H_0\}$ is upper bounded by a user-specified $\alpha \in (0, 1)$. If we knew the cdf of $t(\mathbf{X})$ under H_0 , then we could compute the p-value $\mathbf{q}(t) \triangleq \Pr\{t(\mathbf{X}) \leq t | H_0\}$, which is essentially a way of transforming the random variable $t(\mathbf{X})$ to a new random variable $\mathbf{q}(t(\mathbf{X}))$ that is uniform on $[0, 1]$ under H_0 . In this case, the test $\mathbf{q}(t(\mathbf{x})) \leq \alpha$ would yield a false-alarm rate of α .

When the cdf of $t(\mathbf{X})$ under H_0 is unknown, however, the above procedure cannot be used. An alternative is to replace the p-value $\mathbf{q}(t)$ by the *conformal p-value*

$$\hat{\mathbf{q}}(t) \triangleq \frac{1 + |\{\mathbf{x}_i \in \mathcal{X}_{\text{val}} : t(\mathbf{x}_i) \leq t\}|}{1 + v}, \quad (22)$$

which is computed using a size- v validation set \mathcal{X}_{val} drawn i.i.d. under H_0 and independent of \mathbf{x} and any data used to design $t(\cdot)$. In this case, it's known (Vovk, 2012) that

$$\mathbb{E}[\Pr\{\hat{\mathbf{q}}(t(\mathbf{X})) \leq \mathbf{a} | H_0, \mathcal{X}_{\text{val}}\}] \leq \mathbf{a} \text{ for all } \mathbf{a} \in (0, 1), \quad (23)$$

where the expectation is taken over \mathcal{X}_{val} . Thus, when averaged over *many* validation sets \mathcal{X}_{val} , the test “ $\hat{\mathbf{q}}(t(\mathbf{x})) \leq \alpha$ ” provides a false-alarm rate of α . But in practice we have only *one* validation set, and so this average-case result does not apply.

Our approach is to choose a more conservative threshold “ \mathbf{a} ” on $\hat{\mathbf{q}}(t(\mathbf{x}))$ such that, with probability at least $1 - \delta$, a false-alarm rate of at most α will be attained. To do this, we treat \mathcal{X}_{val} as random, in which case the false-alarm rate $\Pr\{\hat{\mathbf{q}}(t(\mathbf{X})) \leq \mathbf{a} | H_0, \mathcal{X}_{\text{val}}\}$ is itself random and distributed as (Vovk, 2012)

$$\Pr\{\hat{\mathbf{q}}(t(\mathbf{X})) \leq \mathbf{a} | H_0, \mathcal{X}_{\text{val}}\} \sim \text{beta}([\lfloor (v+1)\mathbf{a} \rfloor, v+1 - \lfloor (v+1)\mathbf{a} \rfloor]), \quad (24)$$

which concentrates at \mathbf{a} as the validation size $v \rightarrow \infty$ (Vovk, 2012). Given this distribution, we propose to use bisection search to find a value of \mathbf{a} that guarantees $\alpha_\delta \leq \alpha$, where α_δ is the false-alarm-rate value that yields a beta upper-tail probability of exactly δ .

A procedure to find this \mathbf{a} is given in Algorithm 2, but a few comments are in order. First notice that, due to the floor operations in (24), there exist half-open intervals of \mathbf{a} that yield the same beta parameters and thus the same false-alarm rate statistics. These half-open intervals take the form of $[\frac{l}{v+1}, \frac{l+1}{v+1})$ for $l = 0, \dots, v$. Thus it suffices for the bisection algorithm to find a pair $(\mathbf{a}_{\min}, \mathbf{a}_{\max})$ such that $\mathbf{a}_{\min} \in [\frac{l}{v+1}, \frac{l+1}{v+1})$ yields false-alarm rate $\alpha_{\min} < \alpha$ with probability at least $1 - \delta$, and $\mathbf{a}_{\max} \in [\frac{l+1}{v+1}, \frac{l+2}{v+1})$ yields false-alarm rate $\alpha_{\max} > \alpha$ with probability at least $1 - \delta$, for some $l \in \{0, \dots, v-1\}$. For that value of l , it then suffices to choose any $\mathbf{a} \in [\frac{l}{v+1}, \frac{l+1}{v+1})$, and Algorithm 2 chooses a value close to the right boundary of the interval. The achieved false-alarm rate is then $\alpha_{\min} \triangleq \text{inv cdf}(1 - \delta, \text{beta}(l, v+1-l))$. Figure 3 shows examples of the beta pdf and α_{\min} for validation sizes $v \in \{100, 1000, 10000\}$.

Finally, Algorithm 3 summarizes how conformal p-values can be used for OOD detection while guaranteeing a false-alarm rate of at most α with probability at least $1 - \delta$.

Algorithm 2 Bisection search to find a conformal-p-value threshold of a that yields a false-alarm rate of α with probability at least $1 - \delta$

Require: validation size $v = |\mathcal{X}_{\text{val}}|$, maximum false-alarm rate $\alpha \in (0, 1)$, maximum failure rate $\delta \in (0, 1)$.

- 1: Initialize $\mathbf{a}_{\min} = 0, \mathbf{a}_{\max} = 1$.
 - 2: **while** $\lfloor (v + 1)\mathbf{a}_{\max} \rfloor - \lfloor (v + 1)\mathbf{a}_{\min} \rfloor > 1$ **do**
 - 3: $\mathbf{a} = 0.5(\mathbf{a}_{\min} + \mathbf{a}_{\max})$
 - 4: $l = \lfloor (v + 1)\mathbf{a} \rfloor$
 - 5: $\alpha_\delta = \text{inv cdf}(1 - \delta, \text{beta}(l, v + 1 - l))$
 - 6: **if** $\alpha_\delta > \alpha$ **then**
 - 7: $\mathbf{a}_{\max} = \mathbf{a}$
 - 8: **else**
 - 9: $\mathbf{a}_{\min} = \mathbf{a}$
 - 10: **end if**
 - 11: **end while**
 - 12: **return** $\mathbf{a} = \frac{l+0.99}{v+1}$
-

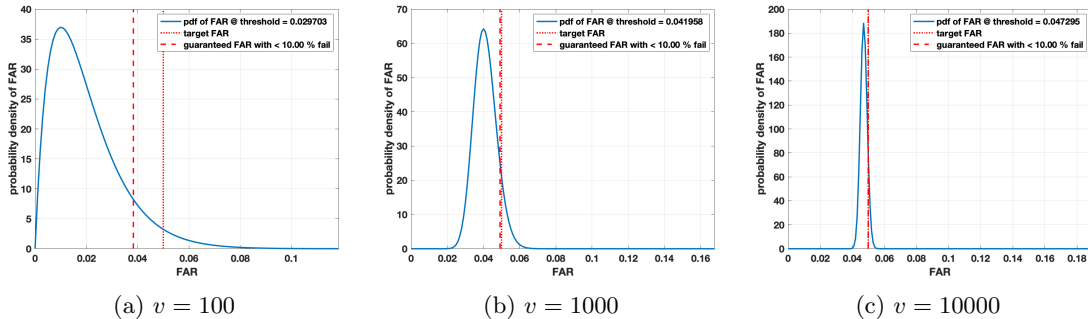


Figure 3: Examples of the beta pdf from (24) and thresholds \mathbf{a} that guarantee a target false-alarm rate (FAR) of at most $\alpha = 0.05$ (red dotted line) with failure probability of at most $\delta = 0.1$. The achieved false alarm rate, α_{\min} , is shown by the dashed red line.

3.4 Using the GLRT for self-supervised OOD detection

As discussed in Section 2.1, many self-supervised OOD detectors compute intermediate scores using pretext tasks, augmented views, and/or distributions shifts, and then combine them heuristically (Golan and El-Yaniv, 2018; Hendrycks et al., 2019b; Bergman and Hoshen, 2020; Tack et al., 2020; Georgescu et al., 2021; Khalid et al., 2022). We instead propose to combine these scores using our GLRT technique. Although our approach could in principle be used to combine any set of inlier scores, we focus on the scores generated by the contrastive CSI and SupCSI techniques from (Tack et al., 2020) due to their state-of-the-art performance.

As described in Section 2.1, CSI (Tack et al., 2020) uses three “base” score functions, $s_{\text{cos},j}(\cdot)$, $s_{\text{norm},j}(\cdot)$, and $s_{\text{shift},j}(\cdot)$, evaluating each on $|\mathcal{T}| = 4$ shifts and combining the 12 resulting scores using the heuristic in (6). We propose to instead combine these 12 scores using the GLRT approach from Section 3.1. We will refer to this latter approach as “glrt-CSI.”

Algorithm 3 OOD detection achieving a false-alarm rate of at most α with probability at least $1 - \delta$

Require: test sample \mathbf{x} , generic inlier test $t(\cdot)$, validation \mathcal{X}_{val} of size v , $\alpha \in (0, 1)$, $\delta \in (0, 1)$.

- 1: Use Algorithm 2 to find $\mathbf{a} \in (0, 1)$ such that $\Pr\{\text{beta}(\lfloor (v+1)\mathbf{a} \rfloor, v+1 - \lfloor (v+1)\mathbf{a} \rfloor) \leq \alpha\} \geq 1 - \delta$
 - 2: Compute the conformal p-value $\widehat{\mathbf{q}}(\mathbf{x}) = \frac{1 + |\{\mathbf{x}_i \in \mathcal{X}_{\text{val}} : t(\mathbf{x}_i) \leq t(\mathbf{x})\}|}{1 + v}$
 - 3: **return** “OOD” if $\widehat{\mathbf{q}}(\mathbf{x}) \leq \mathbf{a}$, else “inlier.”
-

In the case where the inliers have class labels, one can use SupCSI (Tack et al., 2020) to outperform CSI. SupCSI’s score (8) ensembles the logits $\ell(\cdot) \in \mathbb{R}^{K \times |\mathcal{T}|}$ of a joint class/shift classifier head across the $|\mathcal{T}|$ shifts before softmax thresholding. We instead propose to compute a separate softmax-thresholding score for each shift j , i.e.,

$$s_{\text{supCSI},j}(\mathbf{x}) \triangleq \max_{k=1,\dots,K} [\text{softmax}(\ell_{:,j}(R_j(\mathbf{x})))]_k, \quad j = 1 \dots |\mathcal{T}|, \quad (25)$$

and combine them using the GLRT approach from Section 3.1, yielding what we call “glrt-SupCSI.”

Finally, we propose a method that GLRT-combines the CSI and SupCSI base scores, in addition to incorporating two additional base scores: i) one based on supervised OC-SVM

$$s_{\text{supOCSVM},j}(\mathbf{x}) \triangleq \max_{k=1,\dots,K} \left[\sum_{\mathbf{x}_i \in \mathcal{X}_{\text{train},k}} \alpha_{kji} \kappa(f_{\boldsymbol{\theta}}(R_j(\mathbf{x}_i)), f_{\boldsymbol{\theta}}(R_j(\mathbf{x}))) - \rho_{kj} \right], \quad (26)$$

where $\kappa(\mathbf{g}, \mathbf{g}') \triangleq e^{-\gamma \|\mathbf{g} - \mathbf{g}'\|^2}$ is the radial basis function kernel and $\{\alpha_{kji}\}$ and ρ_{kj} are parameters trained on $R_j(\mathbf{x}_i)$ for the class- k subset of $\mathbf{x}_i \in \mathcal{X}_{\text{train}}$, and ii) one based on supervised Mahalanobis

$$s_{\text{supMah},j}(\mathbf{x}) \triangleq - \min_{k=1,\dots,K} \left[(h_{\boldsymbol{\theta}}(R_j(\mathbf{x})) - \widehat{\boldsymbol{\mu}}_{kj}) \widehat{\boldsymbol{\Sigma}}_{kj}^{-1} (h_{\boldsymbol{\theta}}(R_j(\mathbf{x})) - \widehat{\boldsymbol{\mu}}_{kj}) + \log |\widehat{\boldsymbol{\Sigma}}_{kj}| \right], \quad (27)$$

for $j = 1, \dots, |\mathcal{T}|$, where $h_{\boldsymbol{\theta}}(\cdot)$ is the penultimate layer of a ResNet18 trained (with label smoothing (Szegedy et al., 2016)) to jointly classify the shift $j \in \mathcal{T}$ and inlier class k . We found that using this network to compute $s_{\text{supMah},j}$ worked slightly better than using the SupCSI network. In (27), $\widehat{\boldsymbol{\mu}}_{kj}$ and $\widehat{\boldsymbol{\Sigma}}_{kj}$ are the sample mean and covariance of $\{h_{\boldsymbol{\theta}}(R_j(\mathbf{x}_i))\}$ for $\{\mathbf{x}_i\}$ in the class- k subset of $\mathcal{X}_{\text{train}}$. This latter approach, which combines 24 scores in total, is called “glrt-SupCSI+.” See Table 1 for a summary.

4 Experimental results

We now present experimental results comparing our proposed GLRT-based methods to CSI and SupCSI from (Tack et al., 2020) using image data. For the case where the inliers have class labels, we compare to two additional baselines: the softmax-thresholding approach from (Hendrycks and Gimpel, 2017) and the Mahalanobis-based approach from (Lee et al.,

Table 1: Self-supervised OOD detectors and their base scores

Method	Base Scores						Combining	
	$s_{\text{cos},j}$	$s_{\text{norm},j}$	$s_{\text{shift},j}$	$s_{\text{supCSI},j}$	$s_{\text{supOCSVM},j}$	$s_{\text{supMah},j}$	Heuristic	GLRT
CSI	✓	✓	✓				✓	
glrt-CSI	✓	✓	✓					✓
SupCSI				✓			✓	
glrt-SupCSI				✓				✓
glrt-SupCSI+	✓	✓	✓	✓	✓	✓		✓

2018), which both use a supervised classification DNN trained using cross-entropy loss. In addition, we compare our GLRT-based score-combining method to the traditional score-combining methods of Fisher, Bonferroni, Simes/BH, Stouffer, and ALR (Walther, 2013) using the SupCSI+ configuration.

In the subsections below, we focus on two OOD-detection tasks. In the standard “dataset-vs-dataset” task, the inliers are defined by one dataset (e.g., CIFAR-10) and the novelties are defined by a different dataset (e.g., SVHN). For this task, we evaluate 8 different inlier/novelty combinations. In the “leave-one-class-out” task, the inliers are defined by 9 classes of CIFAR-10 and the novelties are defined by the remaining 10th class. This latter task is considered to be much more practically relevant (Ahmed and Courville, 2020) than the dataset-vs-dataset task or the “leave-one-class-in” task, where the inliers are defined by 1 class and the novelties by the remaining 9 classes. To evaluate performance, we will consider both detection rate (DR) for a fixed false-alarm rate (FAR), as well as the area under the receiver operating curve (AUROC), i.e., area under the DR-versus-FAR curve. For the DR-versus-FAR experiments, we used the minimal detection threshold τ under which $\alpha_{\text{test}}(\tau) \leq \alpha$, where α is the target FAR and $\alpha_{\text{test}}(\tau)$ is the FAR measured on the test set.

4.1 Implementation details

First we describe the training of the four DNNs used respectively for CSI, SupCSI, joint class/shift classification (for $s_{\text{supMah},j}$), and supervised classification. All models use the ResNet18 architecture (He et al., 2016) for feature encoding. CSI and SupCSI are trained using the authors’ code under default parameter settings. The joint classifier network is trained using cross-entropy loss with label smoothing (Szegedy et al., 2016) and joint class-shift labels. Finally, the supervised classification network is trained using cross-entropy loss with inlier class labels and without the use of distributional shifting transforms. All networks are trained for 100 epochs using the LARS (You et al., 2017) optimizer. The learning rate is scheduled using cosine annealing (Smith and Topin, 2019) with initial value 0.1, max value 1.0, one epoch of warmup, and a final value of 10^{-6} . The batch size is 128.

4.2 Choice of ϵ

We first consider the choice of ϵ in the NM problem (15) on which our GLRT is based. Figure 4 shows AUROC versus ϵ for the specific task of distinguishing CIFAR-100 novelties from CIFAR-10 inliers. There it can be seen that values of $\epsilon \in (0, 1)$ slightly outperform

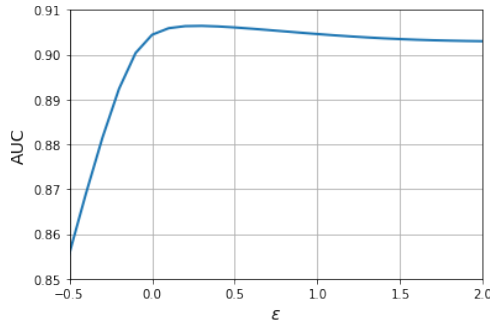


Figure 4: AUROC of glrt-SupCSI+ vs. GLRT parameter ϵ for CIFAR-10 inliers and CIFAR-100 novelties.

the conventional choice (Wei et al., 2019) of $\epsilon = 0$ for this combination of task and metric. Although better performance could be achieved by individually optimizing ϵ for each combination of the 18 tasks and two metrics (DR and AUROC) that we consider, doing would require access to OOD data that is unavailable in practice. Thus, we use $\epsilon = 0.25$ in all cases.

4.3 Dataset-vs-dataset experiments

In this section, we consider experiments where i) the inliers are CIFAR-10 (Krizhevsky, 2009) and the novelties are either SVHN (Netzer et al., 2011), LSUN (Yu et al., 2015), ImageNet (Deng et al., 2009), or CIFAR-100 (Krizhevsky, 2009), and ii) where the inliers are SVHN and the novelties are either LSUN, ImageNet, CIFAR-10, or CIFAR-100. The OOD detectors are trained using the training fold of the inlier dataset and tested using the testing folds of the inlier and novelty datasets.

Tables 2-3 show AUROC for several techniques, while Tables 4-5 show DR for a fixed FAR of 5%. In all of these tables, the techniques above the horizontal line (i.e., CSI and glrt-CSI) have no access to inlier class labels, while the techniques below the horizontal line do. The tables show the contrastive CSI and SupCSI techniques outperforming the softmax-thresholding and Mahalanobis baselines noticeably in AUROC, and drastically in DR, consistent with the existing literature (e.g., (Tack et al., 2020)). The tables also show the proposed glrt-CSI and glrt-SupCSI outperforming their CSI and SupCSI counterparts on average in both AUROC and DR. This demonstrates the advantage of GLRT score-combining over the heuristic combining in (6)-(8). Finally, the tables show that, compared to glrt-SupCSI, the proposed glrt-SupCSI+ does significantly better in DR for CIFAR-10 inliers, slightly better in AUROC in both experiments, and slightly worse in DR for SVHN inliers. This shows that incorporating additional scores *can* be very advantageous, but is not guaranteed to be. We will discuss this phenomenon further in the context of the leave-one-out experiments.

Tables 6-9 compare the proposed GLRT to several existing score-combining rules using the AUROC and DR metrics, respectively. In terms of AUROC, Tables 6-7 show the GLRT outperforming all other methods on average, with Fisher and Stouffer close behind and the other methods performing much worse. In terms of DR, Table 8 shows that, with CIFAR-10 inliers, Stouffer’s method wins and the GLRT and Fisher tie for a close 2nd place,

Table 2: Dataset-vs-dataset AUROC for CIFAR-10 inliers

Method	Novelty Dataset				Avg.
	SVHN	LSUN	ImageNet	CIFAR-100	
CSI	0.9950	0.9750	0.9783	0.8628	0.9528
glrt-CSI	0.9947	0.9768	0.9784	0.8709	0.9552
Softmax	0.9637	0.9015	0.9006	0.8643	0.9075
Mah	0.6063	0.5767	0.4688	0.6923	0.5860
SupCSI	0.9844	0.9787	0.9788	0.9191	0.9652
glrt-SupCSI	0.9863	0.9808	0.9812	0.9214	0.9674
glrt-SupCSI+	0.9968	0.9836	0.9840	0.9064	0.9677

Table 3: Dataset-vs-dataset AUROC for SVHN inliers

Method	Novelty Dataset				Avg.
	LSUN	ImageNet	CIFAR-10	CIFAR-100	
CSI	0.9571	0.9631	0.9638	0.9556	0.9599
glrt-CSI	0.9776	0.9808	0.9677	0.9577	0.9710
Softmax	0.9310	0.9364	0.9346	0.9274	0.9324
Mah	0.9532	0.9616	0.9427	0.9397	0.9493
SupCSI	0.9882	0.9904	0.9909	0.9860	0.9889
glrt-SupCSI	0.9917	0.9929	0.9930	0.9887	0.9916
glrt-SupCSI+	0.9945	0.9952	0.9927	0.9887	0.9928

Table 4: Dataset-vs-dataset detection rate (%) at a false-alarm rate of 5% for CIFAR-10 inliers

Method	Novelty Dataset				Avg.
	SVHN	LSUN	ImageNet	CIFAR-100	
CSI	98.6	87.4	90.1	45.3	80.4
glrt-CSI	98.2	90.9	92.0	45.2	81.6
Softmax	74.9	40.6	38.7	32.6	46.7
Maha	11.7	5.1	4.3	21.2	10.6
SupCSI	91.9	88.5	89.5	59.8	82.4
glrt-SupCSI	92.7	89.6	90.3	57.6	82.6
glrt-SupCSI+	99.3	95.4	95.7	54.3	86.2

while Table 9 shows that, with SVHN inliers, the GLRT and Fisher tie for 1st place while Stouffer is close behind. All together, for the dataset-vs-dataset experiments, the GLRT shows a slight advantage over Fisher and Stouffer and a major advantage over Bonferroni, Simes/BH, and ALR.

4.4 Leave-one-class-out experiments

We now consider experiments where the inliers are 9 classes of CIFAR-10 and the novelties are the remaining class. All 10 configurations are considered under both the AUROC and

Table 5: Dataset-vs-dataset detection rate (%) at a false-alarm rate of 5% for SVHN inliers

Method	Novelty Dataset				Avg.
	LSUN	ImageNet	CIFAR-10	CIFAR-100	
CSI	70.0	76.5	78.8	74.6	75.0
glrt-CSI	89.5	91.7	81.6	75.9	84.7
Softmax	58.6	62.5	62.8	61.7	61.4
Maha	70.0	76.3	61.9	62.0	67.6
SupCSI	97.1	98.2	97.9	94.4	96.9
glrt-SupCSI	98.4	99.0	98.7	95.8	98.0
glrt-SupCSI+	99.3	99.2	97.7	94.9	97.8

Table 6: Dataset-vs-dataset AUROC of SupCSI+ with different score-combining techniques and CIFAR-10 inliers

Method	Novelty Dataset				Avg.
	SVHN	LSUN	ImageNet	CIFAR-100	
GLRT	0.9968	0.9836	0.9840	0.9064	0.9677
Fisher	0.9973	0.9839	0.9838	0.9031	0.9670
Bonferroni	0.9833	0.9719	0.9759	0.8906	0.9554
Simes/BH	0.9837	0.9730	0.9767	0.8920	0.9564
ALR	0.9959	0.9591	0.9541	0.8282	0.9343
Stouffer	0.9976	0.9842	0.9830	0.9033	0.9670

Table 7: Dataset-vs-dataset AUROC of SupCSI+ with different score-combining techniques and SVHN inliers

Method	Novelty Dataset				Avg.
	LSUN	ImageNet	CIFAR-10	CIFAR-100	
GLRT	0.9945	0.9952	0.9927	0.9887	0.9928
Fisher	0.9942	0.9950	0.9925	0.9887	0.9926
Bonferroni	0.9928	0.9929	0.9865	0.9811	0.9883
Simes/BH	0.9929	0.9931	0.9873	0.9823	0.9889
ALR	0.8331	0.8462	0.9047	0.9146	0.8747
Stouffer	0.9929	0.9939	0.9916	0.9880	0.9916

DR metrics. The standard CIFAR-10 train and test folds are used for training and testing, respectively.

Table 10 shows AUROC for several techniques, while Table 11 shows DR for a fixed FAR of 25%. (The FAR was increased to yield meaningful DR values.) The tables show SupCSI outperforming the softmax-thresholding and Mahalanobis baselines noticeably in both AUROC and DR. They also show the proposed glrt-CSI and glrt-SupCSI outperforming their CSI and SupCSI counterparts on average in both AUROC and DR, demonstrating the advantage of GLRT combining. However, the tables show glrt-SupCSI+ underperforming glrt-SupCSI, and even SupCSI, in both AUROC and DR. This is explained by Table 12, which shows that, among the base scores, $s_{\text{supCSI},j}$ has by far the highest AUROC

Table 8: Dataset-vs-dataset detection rate (%) at a false alarm rate of 5% for SupCSI+ with different score-combining techniques and CIFAR-10 inliers

Method	Novelty Dataset				Avg.
	SVHN	LSUN	ImageNet	CIFAR-100	
GLRT	99.3	95.4	95.7	54.3	86.2
Fisher	99.3	95.5	95.7	54.4	86.2
Bonferroni	96.0	86.3	89.5	45.1	79.2
Simes/BH	96.6	87.6	90.3	45.8	80.1
ALR	97.9	86.3	79.6	44.6	77.1
Stouffer	99.4	95.5	95.7	54.6	86.3

Table 9: Dataset-vs-dataset detection rate (%) at a false alarm rate of 5% for SupCSI+ with different score-combining techniques and SVHN inliers

Method	Novelty Dataset				Avg.
	LSUN	ImageNet	CIFAR-10	CIFAR-100	
GLRT	99.3	99.2	97.7	94.9	97.8
Fisher	99.4	99.2	97.7	94.9	97.8
Bonferroni	98.4	98.3	93.5	89.3	94.9
Simes/BH	98.4	98.4	94.2	89.9	95.2
ALR	38.6	44.6	54.5	59.0	49.2
Stouffer	99.4	99.1	97.3	94.5	97.6

Table 10: Leave-one-class-out AUROC

Method	CIFAR-10 Novelty Class										Avg.
	Plane	Car	Bird	Cat	Deer	Dog	Frog	Horse	Ship	Truck	
CSI	0.8230	0.4279	0.8989	0.8889	0.7582	0.7950	0.9298	0.5893	0.6983	0.5876	0.7397
glrt-CSI	0.8185	0.4385	0.8971	0.8941	0.7577	0.8008	0.9181	0.6362	0.6765	0.5835	0.7421
Softmax	0.8304	0.6034	0.8528	0.8503	0.8621	0.8301	0.8669	0.8167	0.7727	0.7199	0.8005
Maha	0.7321	0.6720	0.6943	0.7746	0.5714	0.7078	0.4909	0.7661	0.6694	0.6981	0.6777
SupCSI	0.8827	0.5851	0.9437	0.9026	0.9231	0.8793	0.9690	0.8514	0.7913	0.6406	0.8369
glrt-SupCSI	0.8866	0.5971	0.9448	0.9100	0.9299	0.8729	0.9704	0.8474	0.8186	0.6745	0.8452
glrt-SupCSI+	0.8768	0.6099	0.9270	0.9121	0.8511	0.8427	0.9426	0.8151	0.7497	0.7121	0.8239

in these leave-one-out experiments. Thus, combining $s_{\text{SupCSI},j}$ with other base scores (as in glrt-SupCSI+) leads to lower performance than with $s_{\text{SupCSI},j}$ alone (as in SupCSI and glrt-SupCSI).

Tables 13 and 14 compare the proposed GLRT to several existing score-combining rules using the AUROC and DR metrics, respectively. Both tables show the GLRT outperforming all other methods on average. The other methods perform similarly, except for the ALR (Walther, 2013), which performs noticeably worse.

5 Conclusion

State-of-the-art self-supervised OOD detectors generate several intermediate scores using pretext tasks, augmented views, and/or distribution shifts, and then heuristically combine

Table 11: Leave-one-class-out detection rate (%) at a fixed false alarm rate of 25%

Method	CIFAR-10 Novelty Class										Avg.
	Plane	Car	Bird	Cat	Deer	Dog	Frog	Horse	Ship	Truck	
CSI	73.6	13.5	89.8	87.8	62.4	68.4	97.2	33.7	45.6	30.8	60.3
glrt-CSI	73.5	15.6	89.0	88.3	61.3	68.1	95.8	41.1	42.7	32.2	60.7
Softmax	76.6	36.9	82.8	80.7	86.4	76.2	86.6	74.6	62.2	56.9	72.0
Maha	57.3	46.1	54.1	65.6	29.5	46.8	20.6	62.8	45.9	49.3	47.8
SupCSI	88.8	38.6	96.6	89.7	93.9	89.5	99.8	80.3	70.0	47.5	79.5
glrt-SupCSI	88.7	38.8	96.5	90.7	95.3	87.7	100.	81.8	74.3	48.7	80.3
glrt-SupCSI+	84.4	36.3	93.4	92.1	81.9	81.0	98.9	74.2	56.5	53.1	75.2

Table 12: Leave-one-class-out AUROC for different base scores

Method	CIFAR-10 Novelty Class										Avg.
	Plane	Car	Bird	Cat	Deer	Dog	Frog	Horse	Ship	Truck	
$s_{\text{norm},1}$	0.7481	0.389	0.8308	0.8593	0.7423	0.7641	0.8266	0.6436	0.6873	0.5684	0.7060
$s_{\text{cos},1}$	0.7705	0.4869	0.8479	0.8784	0.7341	0.7992	0.8267	0.7053	0.6366	0.5645	0.7250
$s_{\text{shift},1}$	0.8259	0.4405	0.8835	0.8538	0.7302	0.7625	0.9245	0.5406	0.7007	0.5774	0.7240
$s_{\text{supOCSVM},1}$	0.7216	0.5936	0.6418	0.6116	0.5451	0.5315	0.6629	0.5630	0.4702	0.6743	0.6016
$s_{\text{supCSI},1}$	0.8575	0.5868	0.9247	0.8902	0.9024	0.8607	0.9538	0.8198	0.7879	0.6564	0.8240
$s_{\text{supMah},1}$	0.7186	0.7710	0.6900	0.7123	0.5336	0.6180	0.4795	0.7714	0.6692	0.7948	0.6758

Table 13: Leave-one-class-out AUROC of SupCSI+ with different score-combining techniques

Method	CIFAR-10 Novelty Class										Avg.
	Plane	Car	Bird	Cat	Deer	Dog	Frog	Horse	Ship	Truck	
GLRT	0.8768	0.6099	0.9270	0.9121	0.8511	0.8427	0.9426	0.8151	0.7497	0.7120	0.8239
Fisher	0.8707	0.5990	0.9219	0.9112	0.8309	0.8374	0.9373	0.7972	0.7311	0.7105	0.8147
Bonferroni	0.8513	0.6413	0.9150	0.8760	0.8688	0.7985	0.9383	0.8106	0.7376	0.7191	0.8157
Simes/BH	0.8559	0.6296	0.9189	0.8878	0.8670	0.8127	0.9418	0.8126	0.7367	0.7093	0.8172
ALR	0.8664	0.5993	0.8323	0.8318	0.7264	0.7417	0.7837	0.6589	0.6746	0.7095	0.7425
Stouffer	0.8845	0.5846	0.9250	0.9154	0.8387	0.8507	0.9301	0.7930	0.7575	0.6974	0.8177

Table 14: Leave-one-class-out detection rate (%) at a false-alarm rate of 25% for SupCSI+ with different score-combining techniques

Method	CIFAR-10 Novelty Class										Avg.
	Plane	Car	Bird	Cat	Deer	Dog	Frog	Horse	Ship	Truck	
GLRT	84.4	36.3	93.4	92.1	81.9	81.0	98.9	74.2	56.5	53.1	75.18
Fisher	83.7	33.1	92.1	91.7	76.1	80.1	98.6	69.8	54.8	53.0	73.3
Bonferroni	81.1	41.5	91.8	84.7	85.4	69.5	95.8	72.5	56.7	54.0	73.3
Simes/BH	81.3	42.1	92.7	87.0	86.0	70.8	97.5	72.3	58.1	55.1	74.3
ALR	82.7	37.1	74.7	74.9	50.1	55.7	63.9	41.7	48.5	60.4	59.0
Stouffer	86.0	33.0	94.1	92.8	77.0	84.8	98.1	66.1	55.3	49.8	73.7

them to form a final inlier score. We proposed a principled approach to score combining based on null-hypothesis testing. In particular, we posed the non-negative means problem (15), solved it using a GLRT, and used that GLRT to combine the intermediate scores of the CSI and SupCSI techniques, as well as additional scores. We also proposed an extension that uses a validation dataset to achieve probabilistic guarantees on the false-alarm rate. Both dataset-vs-dataset experiments and leave-one-class-out experiments showed that our GLRT-based approach outperformed the state-of-the-art CSI and SupCSI methods (Tack

et al., 2020) in both AUROC and detection rate for a fixed false-alarm rate. In addition, our GLRT-based approach outperformed the traditional score-combining methods of Fisher, Bonferroni, Simes/BH, Stouffer, and ALR for our OOD detection tasks.

Limitations. One limitation of our approach is that, given a set of base scores, it is not clear which to combine. Our experiments showed that, in some cases, incorporating additional scores reduced performance. Another limitation of our approach is that it builds on self-supervised methods that rely on a set of transformations \mathcal{T} . For images, good transformations are known, but for other modalities (e.g., audio or tabular data) it is not clear which transformations to use.

Acknowledgments and Disclosure of Funding

This work was supported in part by the National Science Foundation under grant 1539961 and the Air Force Research Laboratory under grant FA8650-32-C-1174. This work has been cleared for public release via PA Approval number AFRL-2023-2205.

References

- F. Ahmed and A. Courville. Detecting semantic anomalies. In *Proc. AAAI Conf. Artificial Intell.*, volume 34, pages 3154–3162, 2020.
- M. S. Anderson, J. Dahl, and L. Vandenberghe. CVXOPT: A python package for convex optimization, 2012. URL abel.ee.ucla.edu/cvxopt.
- Y. Benjamini and Y. Hochberg. Controlling the false discovery rate: a practical and powerful approach to multiple testing. *J. Roy. Statist. Soc. B*, 57(1):289–300, 1995.
- F. Bergamin, P.-A. Mattei, J. D. Havtorn, H. Senetaire, H. Schmutz, L. Maaløe, S. Hauberg, and J. Frellsen. Model-agnostic out-of-distribution detection using combined statistical tests. In *Proc. Intl. Conf. Artificial Intell. Statist.*, pages 10753–10776, 2022.
- L. Bergman and Y. Hoshen. Classification-based anomaly detection for general data. In *Proc. Intl. Conf. Learn. Rep.*, 2020.
- R. H. Berk and D. H. Jones. Goodness-of-fit test statistics that dominate the Kolmogorov statistics. *Zeitschrift für Wahrscheinlichkeitstheorie und verwandte Gebiete*, 47(1):47–59, 1979.
- C. M. Bishop. Novelty detection and neural network validation. *IEE Proc. V: Vision, Image & Signal Process.*, 141(4):217–222, 1994.
- M. M. Breunig, H.-P. Kriegel, R. T. Ng, and J. Sander. LOF: Identifying density-based local outliers. In *Proc. ACM SIGMOD Intl. Conf. Manag. Data*, pages 93–104, 2000.
- R. Chalapathy and S. Chawla. Deep learning for anomaly detection: A survey. *arXiv:1901.03407*, 2019.
- T. Chen, S. Kornblith, M. Norouzi, and G. Hinton. A simple framework for contrastive learning of visual representations. In *Proc. Intl. Conf. Mach. Learn.*, pages 1597–1607, 2020.
- R. D. Cousins. Annotated bibliography of some papers on combining significances or p-values. *arXiv:0705.2209*, 2007.
- L. Deecke, L. Ruff, R. Vandermeulen, and H. Bilen. Transfer-based semantic anomaly detection. In *Proc. Intl. Conf. Mach. Learn.*, pages 2546–2558, 2021.
- J. Deng, W. Dong, R. Socher, L.-J. Li, K. Li, and L. Fei-Fei. Imagenet: A large-scale hierarchical image database. In *Proc. IEEE Conf. Comp. Vision Pattern Recog.*, pages 248–255, 2009.
- F. Di Mattia, P. Galeone, M. De Simoni, and E. Ghelfi. A survey on GANs for anomaly detection. *arXiv:1906.11632*, 2019.
- D. Donoho and J. Jin. Higher criticism for detecting sparse heterogeneous mixtures. *Ann. Statist.*, 32(3):962–994, 2004.

- L. Ericsson, H. Gouk, C. C. Loy, and T. M. Hospedales. Self-supervised representation learning: Introduction, advances, and challenges. *IEEE Signal Process. Mag.*, 39(3): 42–62, 2022.
- R. A. Fisher. *Statistical methods for research workers*. Springer, 1992.
- M.-I. Georgescu, A. Barbalau, R. T. Ionescu, F. S. Khan, M. Popescu, and M. Shah. Anomaly detection in video via self-supervised and multi-task learning. In *Proc. IEEE Conf. Comp. Vision Pattern Recog.*, pages 12742–12752, 2021.
- S. Gidaris, P. Singh, and N. Komodakis. Unsupervised representation learning by predicting image rotations. In *Proc. Intl. Conf. Learn. Rep.*, Apr. 2018.
- I. Golan and R. El-Yaniv. Deep anomaly detection using geometric transformations. In *Proc. Neural Info. Process. Syst. Conf.*, volume 31, 2018.
- M. Haroush, T. Frostig, R. Heller, and D. Soudry. A statistical framework for efficient out of distribution detection in deep neural networks. In *Proc. Intl. Conf. Learn. Rep.*, 2022.
- K. He, X. Zhang, S. Ren, and J. Sun. Deep residual learning for image recognition. In *Proc. IEEE Conf. Comp. Vision Pattern Recog.*, pages 770–778, 2016.
- D. Hendrycks and K. Gimpel. A baseline for detecting misclassified and out-of-distribution examples in neural networks. In *Proc. Intl. Conf. Learn. Rep.*, 2017.
- D. Hendrycks, M. Mazeika, and T. Dietterich. Deep anomaly detection with outlier exposure. In *Proc. Intl. Conf. Learn. Rep.*, 2019a.
- D. Hendrycks, M. Mazeika, S. Kadavath, and D. Song. Using self-supervised learning can improve robustness and uncertainty. In *Proc. Neural Info. Process. Syst. Conf.*, 2019b.
- H. Hoffmann. Kernel PCA for novelty detection. *Pattern Recognition*, 40(3):863–874, 2007.
- R. Kaur, S. Jha, A. Roy, S. Park, E. Dobriban, O. Sokolsky, and I. Lee. iDECODE: In-distribution equivariance for conformal out-of-distribution detection. In *Proc. AAAI Conf. Artificial Intell.*, volume 36, pages 7104–7114, 2022.
- U. Khalid, A. Esmaili, N. Karim, and N. Rahnavard. RODD: A self-supervised approach for robust out-of-distribution detection. In *Proc. IEEE Conf. Comp. Vision Pattern Recog. Workshop*, pages 163–170, 2022.
- P. Khosla, P. Teterwak, C. Wang, A. Sarna, Y. Tian, P. Isola, A. Maschinot, C. Liu, and D. Krishnan. Supervised contrastive learning. In *Proc. Neural Info. Process. Syst. Conf.*, volume 33, pages 18661–18673, 2020.
- A. Krizhevsky. Learning multiple layers of features from tiny images. *Technical Report*, 2009. URL <https://www.cs.toronto.edu/~kriz/learning-features-2009-TR.pdf>.
- L. J. Latecki, A. Lazarevic, and D. Pokrajac. Outlier detection with kernel density functions. In *Proc. Mach. Learn. Data Mining Pattern Recog.*, volume 7, pages 61–75, 2007.

- J. Laurikkala, M. Juhola, E. Kentala, N. Lavrac, S. Miksch, and B. Kavsek. Informal identification of outliers in medical data. In *Intl. Workshop Intell. Data Anal. Med. Pharma.*, pages 20–24, 2000.
- K. Lee, K. Lee, H. Lee, and J. Shin. A simple unified framework for detecting out-of-distribution samples and adversarial attacks. In *Proc. Neural Info. Process. Syst. Conf.*, 2018.
- E. L. Lehmann, J. P. Romano, and G. Casella. *Testing Statistical Hypotheses*, volume 3. Springer, 2005.
- A. Magesh, V. V. Veeravalli, A. Roy, and S. Jha. Multiple testing framework for out-of-distribution detection. *arXiv:2206.09522*, 2022.
- Y. Netzer, T. Wang, A. Coates, A. Bissacco, B. Wu, and A. Y. Ng. Reading digits in natural images with unsupervised feature learning. In *Proc. Neural Info. Process. Syst. Conf.*, 2011.
- G. Pang, C. Shen, L. Cao, and A. V. D. Hengel. Deep learning for anomaly detection: A review. *ACM Comput. Surveys*, 54(2):1–38, 2021.
- S. Ramaswamy, R. Rastogi, and K. Shim. Efficient algorithms for mining outliers from large data sets. In *Proc. ACM SIGMOD Intl. Conf. Manag. Data*, pages 427–438, 2000.
- T. Reiss and Y. Hoshen. Mean-shifted contrastive loss for anomaly detection. In *Proc. AAAI Conf. Artificial Intell.*, Washington, DC, Feb. 2023.
- T. Reiss, N. Cohen, L. Bergman, and Y. Hoshen. PANDA: Adapting pretrained features for anomaly detection and segmentation. In *Proc. IEEE Conf. Comp. Vision Pattern Recog.*, page 2806–2814, virtual, June 2021.
- L. Ruff, R. Vandermeulen, N. Görnitz, A. Binder, E. Müller, K. Müller, and M. Kloft. Transfer-based semantic anomaly detection. In *Proc. Intl. Conf. Learn. Rep.*, 2020.
- L. Ruff, J. R. Kauffmann, and R. A. Vandermeulen. A unifying review of deep and shallow anomaly detection. *Proc. IEEE*, 109(5):756–795, 2021.
- B. Schölkopf, J. C. Platt, J. C. Shawe-Taylor, A. J. Smola, and R. C. Williamson. Estimating the support of a high-dimensional distribution. *Neural Comput.*, 13(7):1443–1471, July 2001.
- R. J. Simes. An improved Bonferroni procedure for multiple tests of significance. *Biometrika*, 73(3):751–754, 1986.
- L. N. Smith and N. Topin. Super-convergence: Very fast training of neural networks using large learning rate. In T. Pham, editor, *Artificial Intell. Machine Learning for Multi-Domain Operations Applications*, volume 11006, page 11006 12. SPIE, 2019.
- K. Sohn, C.-L. Li, J. Yoon, M. Jin, and T. Pfister. Learning and evaluating representations for deep one-class classification. In *Proc. Intl. Conf. Learn. Rep.*, 2021.

- C. Szegedy, V. Vanhoucke, S. Ioffe, J. Shlens, and Z. Wojna. Rethinking the inception architecture for computer vision. In *Proc. IEEE Conf. Comp. Vision Pattern Recog.*, 2016.
- J. Tack, S. Mo, J. Jeong, and J. Shin. CSI: Novelty detection via contrastive learning on distributionally shifted instances. In *Proc. Neural Info. Process. Syst. Conf.*, pages 11839–11852, 2020.
- D. Tax and R. Duin. Support vector data description. *Mach. Learn.*, 54:45–66, 2004.
- V. Vovk. Conditional validity of inductive conformal predictors. In *Asian Conf. Mach. Learn.*, pages 475–490, 2012.
- G. Walther. The average likelihood ratio for large-scale multiple testing and detecting sparse mixtures. *Inst. Math. Stat.(IMS) Collect*, 9:317–326, 2013.
- T. Wang and P. Isola. Understanding contrastive representation learning through alignment and uniformity on the hypersphere. In *Proc. Intl. Conf. Mach. Learn.*, pages 9929–9939, 2020.
- L. Wasserman. *All of Statistics: A Concise Course in Statistical Inference*. Springer, 2004.
- Y. Wei, M. J. Wainwright, and A. Guntuboyina. The geometry of hypothesis testing over convex cones: Generalized likelihood ratio tests and minimax radii. *Ann. Statist.*, 47(2): 994–1024, 2019.
- J. Winkens, R. Bunel, A. G. Roy, R. Stanforth, V. Natarajan, J. R. Ledsam, P. MacWilliams, P. Kohli, A. Karthikesalingam, S. Kohl, T. Cemgil, S. M. A. Eslami, and O. Ronneberger. Contrastive training for improved out-of-distribution detection. *arXiv:2007.05566v1*, July 2020.
- Y. You, B. Ginsburg, and I. Gitman. Large batch training of convolutional networks. *arXiv:1708.03888v3*, 2017.
- F. Yu, A. Seff, Y. Zhang, S. Song, T. Funkhouser, and J. Xiao. LSUN: Construction of a large-scale image dataset using deep learning with humans in the loop. *arXiv:1506.03365*, 2015.
- A. Zimek, E. Schubert, and H.-P. Kriegel. A survey on unsupervised outlier detection in high-dimensional numerical data. *Stat. Anal. and Data Mining*, 5(5):363–387, 2012.

Appendix A. Alternative formulations

As discussed in Section 3.1, the NM problem (15) models the z-values as independent, even though we don't expect them to be independent in practice. In this appendix, we discuss two alternative formulations that address this independence issue and explain their limitations.

A.1 Multiple hypothesis testing

One way to avoid the independence assumption in (15) is to instead use a *multiple hypothesis testing* formulation (Wasserman, 2004), i.e.,

$$\text{for } l = 1, \dots, m, \quad \begin{cases} H_{0l} : Z_l \sim \mathcal{N}(0, 1) \\ H_{1l} : Z_l \sim \mathcal{N}(\mu_l, 1) \text{ for some } \mu_l \leq -\epsilon, \end{cases} \quad (28)$$

from which the global inlier hypothesis (that $\mathbf{x} \sim P_x$) would be constructed as $H_0 = \cap_{l=1}^m H_{0l}$. But, as we now show, (28) reduces to the classical methods of score combining reviewed in Section 2.2. To see why, recall that the test “ $z_l \leq \tau$ ” is UMP for rejecting H_{0l} . To combine $\{z_l\}_{l=1}^m$, one could use Stouffer's method or convert them to p-values $\bar{q}_l = \Phi(z_l)$ and use a classical p-value combining method like Bonferroni. But since the transformations from the raw score $s_l(\mathbf{x})$ to z_l to \bar{q}_l are all strictly monotonically increasing, the p-value \bar{q}_l will be identical to the p-value q_l computed from the raw score $s_l(\mathbf{x})$, and so (28) reduces to classical score-combining. We numerically compare these classical score-combining approaches to the proposed GLRT in Section 4.

For completeness, we note that the $\epsilon = 0$ case of (28) was briefly discussed by Donoho and Jin in (Donoho and Jin, 2004). For tractability, however, the authors approximated H_{1l} by a Gaussian-mixture model and analyzed it in the sparse regime, which led them to propose the *higher criticism* (HC) statistic. Later, Walther (Walther, 2013) compared the HC statistic to the *Berk-Jones* (BJ) statistic (Berk and Jones, 1979) and found that one or the other may dominate, depending on the sparsity of the mixture. Walther then proposed the *adjusted likelihood ratio* (ALR) statistic and empirically demonstrated that it performs similarly to the best of HC and BJ. We numerically investigate the ALR approach in Section 4.

A.2 The negative-means problem with general covariances

Another way to avoid the independence assumption in (15) is to explicitly model correlation among the z-values via

$$H_0 : \mathbf{Z} \sim \mathcal{N}(\mathbf{0}, \Sigma_0) \quad (29a)$$

$$H_1 : \mathbf{Z} \sim \mathcal{N}(\boldsymbol{\mu}, \Sigma_1) \text{ with } \mu_l \leq -\epsilon \text{ for all } l = 1, \dots, m. \quad (29b)$$

Although Σ_0 could be chosen as the inlier sample-covariance matrix $\widehat{\Sigma}$, it's not clear how to choose Σ_1 since we have no information about the novelties. One possibility is to use the inlier sample-covariance matrix for both Σ_0 and Σ_1 .

Table 15: Dataset-vs-dataset AUROC of SupCSI+ with $\ln \text{GLR}(\mathbf{z}; \mathbf{\Sigma})$ -based score combining for two choices of $\mathbf{\Sigma}$

(a) Inlier dataset - CIFAR-10						(b) Inlier dataset - SVHN					
novelty dataset						novelty dataset					
$\mathbf{\Sigma}$	SVHN	LSUN	ImageNet	CIFAR-100	Avg.	$\mathbf{\Sigma}$	SVHN	LSUN	ImageNet	CIFAR-100	Avg.
$\widehat{\mathbf{\Sigma}}$	0.9712	0.9608	0.9683	0.8239	0.9311	$\widehat{\mathbf{\Sigma}}$	0.9922	0.9917	0.9692	0.9618	0.9787
\mathbf{I}	0.9968	0.9836	0.9840	0.9064	0.9677	\mathbf{I}	0.9945	0.9952	0.9927	0.9887	0.9928

In any case, we will study (29) further under the assumption that $\mathbf{\Sigma}_0 = \mathbf{\Sigma}_1 = \mathbf{\Sigma}$ for some $\mathbf{\Sigma}$. If $\boldsymbol{\mu}$ was known, then the log-LR (recall (16)) would be

$$\log \text{LR} = -\frac{1}{2} \mathbf{z}^\top \mathbf{\Sigma}^{-1} \mathbf{z} + \frac{1}{2} (\mathbf{z} - \boldsymbol{\mu})^\top \mathbf{\Sigma}^{-1} (\mathbf{z} - \boldsymbol{\mu}). \quad (30)$$

Since $\boldsymbol{\mu}$ is unknown, we could pose the GLRT

$$\text{GLR}(\mathbf{z}) \underset{H_1}{\overset{H_0}{\geq}} \tau \quad \text{for} \quad \text{GLR}(\mathbf{z}) = \frac{\mathcal{N}(\mathbf{z}; \mathbf{0}, \mathbf{\Sigma})}{\max_{\boldsymbol{\mu}: \mu_l \leq -\epsilon \forall l} \mathcal{N}(\mathbf{z}; \boldsymbol{\mu}, \mathbf{\Sigma})}, \quad (31)$$

whose denominator is maximized by

$$\boldsymbol{\mu}^* \triangleq \arg \max_{\boldsymbol{\mu}: \mu_l \leq -\epsilon \forall l} \mathcal{N}(\mathbf{z}; \boldsymbol{\mu}, \mathbf{\Sigma}) = \arg \min_{\boldsymbol{\mu}: \mu_l \leq -\epsilon \forall l} (\mathbf{z} - \boldsymbol{\mu})^\top \mathbf{\Sigma}^{-1} (\mathbf{z} - \boldsymbol{\mu}). \quad (32)$$

Since (32) is a quadratic program, $\boldsymbol{\mu}^*$ could be readily computed using an optimization package like CVX (Anderson et al., 2012). Plugging $\boldsymbol{\mu}^*$ into the log-LR expression (30), we obtain

$$\ln \text{GLR}(\mathbf{z}; \mathbf{\Sigma}) = \left(\frac{1}{2} \boldsymbol{\mu}^*(\mathbf{z}) - \mathbf{z} \right)^\top \mathbf{\Sigma}^{-1} \boldsymbol{\mu}^*(\mathbf{z}), \quad (33)$$

which could be used as a test statistic. In particular, we would reject the null hypothesis H_0 whenever $\ln \text{GLR}(\mathbf{z}; \mathbf{\Sigma}) \geq \tau$ for an appropriately chosen threshold τ . In (33), we wrote “ $\boldsymbol{\mu}^*(\mathbf{z})$ ” to emphasize the dependence of $\boldsymbol{\mu}^*$ on \mathbf{z} .

Recall that the proposed $t_{\text{GLRT}}(\mathbf{z})$ in (20) results from using $\ln \text{GLR}(\mathbf{z}; \mathbf{\Sigma})$ with $\mathbf{\Sigma} = \mathbf{I}$. Another choice for $\mathbf{\Sigma}$ would be the inlier covariance, which could be computed from inlier training data $\mathcal{X}_{\text{train}} = \{\mathbf{x}_i\}$ via

$$\widehat{\mathbf{\Sigma}} \triangleq \frac{1}{n-1} \sum_{i=1}^n \mathbf{z}_i \mathbf{z}_i^\top + \sigma \mathbf{I}, \quad (34)$$

where \mathbf{z}_i contains the empirical z-values associated with the training sample \mathbf{x}_i and $\sigma > 0$ is a small constant that ensures $\widehat{\mathbf{\Sigma}}$ is full rank. We use $\sigma = 10^{-6}$ in our experiments.

We now empirically study the choice of $\mathbf{\Sigma}$ in $\ln \text{GLR}(\mathbf{z}; \mathbf{\Sigma})$ by repeating the dataset-vs-dataset experiments from Section 4. Table 15 shows the performance of SupCSI+ with $\ln \text{GLR}(\mathbf{z}; \mathbf{\Sigma})$ -based score combining using $\mathbf{\Sigma} = \mathbf{I}$ versus $\mathbf{\Sigma} = \widehat{\mathbf{\Sigma}}$. There we see that $\mathbf{\Sigma} = \mathbf{I}$ leads to better AUROC performance than $\mathbf{\Sigma} = \widehat{\mathbf{\Sigma}}$ in most experiments, and on average across experiments.

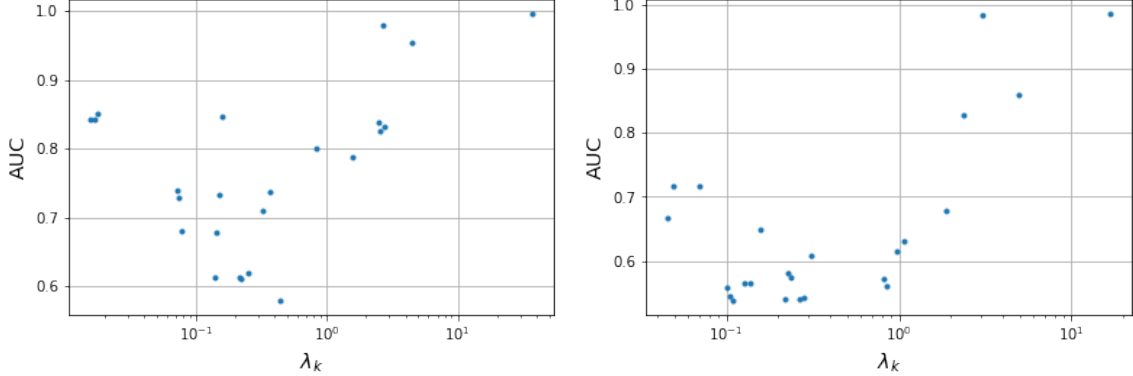


Figure 5: AUROC of eigen-score $t_{\text{eig},k}(\mathbf{z})$ versus eigenvalue λ_k for $k = 1, \dots, m$ on two $m = 24$ score experiments from Section 4: CIFAR-10 inliers with SVHN novelties (left) and SVHN novelties with CIFAR-10 inliers (right).

Next, we perform an eigen-analysis of the log-GLRT score in an attempt to better understand the reason that $\Sigma = \mathbf{I}$ performs better than $\Sigma = \hat{\Sigma}$. We write the eigen-decomposition of the inlier covariance matrix as

$$\hat{\Sigma} = \sum_{k=1}^m \lambda_k \mathbf{v}_k \mathbf{v}_k^\top, \quad (35)$$

where $\{\mathbf{v}_k\}_{k=1}^m$ are orthonormal eigenvectors and $\{\lambda_k\}_{k=1}^m$ are non-negative eigenvalues. The log-GLR from (33) can then be written as

$$\ln \text{GLR}(\mathbf{z}; \hat{\Sigma}) = \sum_{k=1}^m \frac{t_{\text{eig},k}(\mathbf{z})}{\lambda_k} \quad \text{and} \quad \ln \text{GLR}(\mathbf{z}; \mathbf{I}) = \sum_{k=1}^m t_{\text{eig},k}(\mathbf{z}) \quad (36)$$

$$\text{for } t_{\text{eig},k}(\mathbf{z}) \triangleq \left(\frac{1}{2} \boldsymbol{\mu}^*(\mathbf{z}) - \mathbf{z}\right)^\top \mathbf{v}_k \cdot \mathbf{v}_k^\top \boldsymbol{\mu}^*(\mathbf{z}), \quad (37)$$

where the second equality in (36) follows from the fact that $\sum_{k=1}^m \mathbf{v}_k \mathbf{v}_k^\top = \mathbf{I}$.

In Figure 5, we plot the AUROC performance of the ‘‘eigen-score’’ $t_{\text{eig},k}$ versus the eigenvalue λ_k for the two experiments from Table 15. Both experiments show a positive correlation between AUROC performance of the eigen-score $t_{\text{eig},k}(\mathbf{z})$ and the size of the corresponding eigenvalue λ_k . Thus, dividing $t_{\text{eig},k}(\mathbf{z})$ by λ_k , as done when constructing $\ln \text{GLR}(\mathbf{z}; \hat{\Sigma})$, will devalue the better-performing tests. Conversely, not dividing $t_{\text{eig},k}(\mathbf{z})$ by λ_k , as done when constructing $\ln \text{GLR}(\mathbf{z}; \mathbf{I})$, will lead to better performance.